Cement 14 (2023) 100088

Contents lists available at ScienceDirect

Cement

journal homepage: www.sciencedirect.com/journal/cement

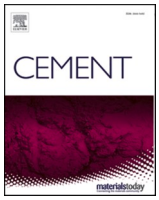

Multiscale performance and environmental impact assessment of slag and Portland blended cement for optimum carbonation curing

Rakibul I. Khan [a,b], Muhammad Intesarul Haque [a], Adhora Tahsin [a], Warda Ashraf [a,*]

[a] Department of Civil Engineering, University of Texas at Arlington, TX, 76010, USA
[b] Laticrete International Inc, Bethany, CT, 06524-3423, USA

ARTICLE INFO

Keywords:
Carbonation curing
Portland cement
Slag cement
Microstructure
Life cycle analysis

ABSTRACT

This article presents an investigation into the potential use of ground granulated blast-furnace slag (addressed as Slag cement or 'SC') as a replacement to Ordinary Portland Cement (OPC) in hybrid (carbonation and hydration) cured cement-based materials. To investigate the effects of carbonation on mechanical performances and microstructures, 0 %–100 % OPC was replaced with slag cement (SC). Thermogravimetric analysis (TGA) and Fourier transformed infrared (FTIR) spectra were utilized to investigate the carbonation reaction extent, rate, and microstructural phase formations. Slag cement was found to improve the efficiency and rate of carbonation. This study revealed that a minimum of 72 h of carbonation in a CO_2-containing environment yields better mechanical performance compared to the traditional curing method. Specifically, the incorporation of 72 h of carbonation curing was observed to increase the strength of concrete up to 30 % after 28 days of total curing duration (carbonation and hydration). The chloride permeability of the carbonation cured samples was observed to reduce by 80 % due to the addition of SC. Finally, it was observed that, the carbonated concrete sample with slag has nearly 60 % lower global warming potential compared to the carbonated and non-carbonated concrete sample with 100 % OPC binder.

1. Introduction

The Ordinary Portland Cement (OPC) industry is the most energy-intensive of all manufacturing industries [1–3]. This industry accounts for 5 %−8 % of global man-made CO_2 emissions [4–7] and 12–15 % of total energy use by the industry [8]. This significant environmental impact resulting from OPC production has paved the way for more investigation into sustainable alternatives to OPC-based construction materials with a low CO_2 footprint. Researchers are investigating the use of mineral admixtures (i.e., wollastonite [9]) or industrial by-products (i.e., coal fly-ash [10], slag cement [11], silica fume [12,13], and metakaolin [12,14]) as supplementary cementitious materials (SCMs) for lower CO_2 emissions. The use of supplementary cementitious materials improves the durability of concrete and has environmental benefits. Recent studies focus on reducing energy consumption while also sequestering CO_2 in the concrete [15–18].

Carbonation (CO_2) curing is acquiring increasing attention and prominence due to its multiple roles in the concrete [19], i.e., sequestrating CO_2 from the environment and providing rapid strength gain of the cementitious materials [19]. Calcium silicates, one of the primary ingredients of cement, react with CO_2 in the presence of water in the carbonation curing system, and form $CaCO_3$ and Ca-modified silica gels as reaction products [20]. During the carbonation curing of hydraulic or semi-hydraulic materials, $Ca(OH)_2$, $CaCO_3$, calcium silicate hydrate (C-S-H), and Ca-modified silica gel are produced, which provide more dense and durable microstructures compared to the traditional concrete [19–21]. This technological innovation is efficient and robust in the sequestration of CO_2 in construction materials [1]. This study also aims to perform life cycle analysis in OPC-slag systems while improving material properties through accelerated carbonation curing.

Slag cement (SC) is a supplementary cementitious material produced as a by-product of the steel industry [22–24]. This semi-hydraulic and calcium-rich amorphous material is found to demonstrate higher carbonation reactivity as it often contains hydraulic calcium silicate (Ca_3SiO_5, β- Ca_2SiO_4), non-hydraulic calcium silicate (γ-Ca_2SiO_4), and portlandite in addition to amorphous calcium-alumina-silica phase [22,25]. SC has latent hydraulic properties and demonstrates longer initial and final setting times [26]. Carbonation curing helps to increase the early strength gain of slag cement. Boone et al. (2014) reported that carbonation of SC significantly reduced pore size distribution and pore

* Corresponding author.
E-mail address: warda.ashraf@uta.edu (W. Ashraf).

https://doi.org/10.1016/j.cement.2023.100088
Received 29 May 2023; Received in revised form 28 October 2023; Accepted 30 November 2023
Available online 1 December 2023

volume [27]. This densification had a considerable influence on compressive strength [22]. Previous studies also discussed that shrinkage of the carbonation-cured mortar containing SC was lower compared to the traditional OPC mortar [28]. The long-term durability of these materials is still being debated. This is one of the most crucial issues to address for gaining acceptance and confidence that these alternative materials can be used in large-scale applications. Accordingly, this present research also explores the durability of a carbonation-cured OPC-slag system.

This study also evaluates the environmental performance by conducting a lifecycle analysis on SimaPro 9.0.0.48. A cradle-to-gate approach was considered, which involves raw materials acquisition, transportation of these materials to the plant, and concrete/ mortar production [29,30]. The Tool for the Reduction and Assessment of Chemical and other environmental Impacts (T.R.A.C.I.) impact assessment method was considered, and several environmental impact categories caused by these binders and mortars were explored. The difference between the environmental impacts of binder and mortar mixes is the inclusion of fine and coarse aggregates in the mortar. Most studies consider mass-based functional units [31,32]. However, one unit mass of one binder may not be functionally equivalent to another unit of another binder. Other parameters like compressive strength and durability can be considered when comparing the functionality of different binders. Some studies considered the cement functional performance (CFP) as a functional unit, which considers the mass of binder needed per m^3 of mortar or concrete for achieving 1 MPa of compressive strength (kg/m^3/ MPa) [33,34]. The functional unit considered in this study was related to the CFP of the produced specimens by using varying binder mixtures.

In this research, a potential hybrid curing (carbonation and hydration) was investigated, and it was discovered that hydration curing prior to carbonation yielded better performance than carbonation and hydration alone. This research also provided information on the environmental impacts of OPC-slag carbonation cured system. The specific objectives of this study were to determine the synergic effects of SC and OPC carbonation on i) carbonation rate, ii) carbonation efficiency, iii) microstructures, iv) silica gel polymerization, v) compressive strength, vi) durability of cement-based materials, and vii) life cycle analysis of carbonation cured OPC-slag system. This study's findings will help to understand the mechanism of SC—OPC interaction in the carbonated system.

2. Materials and methods

2.1. Materials

In this study, the raw materials used are OPC, Ground Granulated Blast Furnace Slag (addressed as 'slag cement' or SC), sand, and gravel. Slag cement (SC) was supplied by Dragon products company, Maine, USA. Based on the X-ray fluorescence measurement, the OPC contained 20.1 % SiO_2, 63.7 % CaO, 4.7 % Al_2O_3, 3.5 % Fe_2O_3, and the SC contained 34.7 % SiO_2, 13.7 % Al_2O_3, 0.9 % Fe_2O_3, 42.3 % CaO, 5.6 % MgO, 1.7 % SO_3. River sand with 2.61 finesse modulus (F.M.) was used as fine aggregates, and gravel was used as coarse aggregates. The particle size analyses of the OPC and Slag Cement (SC) were performed by Malvern Mastersizer 2000 using a 1.63 refractive index and deionized water as a solvent. The mean particle sizes of the OPC and SC were 20 μm and 14 μm, respectively. The distribution of particle size is shown in Fig. 1.

2.2. Sample preparation

Two categories of samples were prepared for this study, as shown in Fig. 2. For the first category, five different paste mixtures were prepared by replacing OPC by 0 %, 45 %, 65 %, 80 %, and 100 % by weight of Ground Granulated Blast Furnace Slag (addressed as 'slag cement' or SC in the remainder of the study). SC and OPC were mixed using a 'Renfert Twister Evolution' mixer with a w/b ratio of 0.40. The ASTM C305 [35] standard was followed during mixing. Thin plate-like (2~3 mm thickness) paste samples were prepared without compaction for microstructural analysis. Those thin plate-like samples were kept in a carbonation chamber (discussed in the next section), and the carbonation reaction throughout the cross-section of the sample was considered uniform. This sample category was used for carbonation reaction kinetics and Fourier Transform-Infrared Spectroscopy (FTIR) measurements. The samples were immersed in ethanol to halt the reaction and eliminate water content. Subsequently, those samples underwent a 48-hour drying period within a vacuum chamber [36]. Following this, TGA and FTIR tests were conducted.

The second category included 100 mm × 200 mm cylindrical concrete samples for mechanical performance and durability testing. This category of samples was prepared for the compressive strength and rapid chloride penetration (RCPT) tests. Six different concrete mix designs were adopted to prepare concrete cylinders using a constant w/b ratio of 0.40. In these samples, OPC was replaced by 0 %, 20 %, 45 %, 65 %, 80 %, and 100 % by weight of SC. For the remainder of this article, the mixer of 100 % OPC or 0 % SC content will be called as the control batch. Concrete mixing was performed in a large mechanical mixer in accordance with the ASTM C192 [37] standard. A fine aggregate and coarse aggregate proportions of 38 % and 62 %, respectively, were used. The binder (OPC + SC) and aggregate contents of the mixtures were 400 kg/m^3 and 1890 kg/m^3, respectively. 100 mm by 200 mm cylinders were prepared for mechanical and durability testing using these samples. The cylinders were prepared in three layers using a mechanical vibrator and a tamping rod. Each layer was vibrated for 45 s for compaction. After casting, the cylinders were kept under different curing conditions, as described in Section 2.3. Cylinders were demolded after 24 h of casting and kept in the previous curing condition.

Slump tests to measure the workability of each batch of concrete

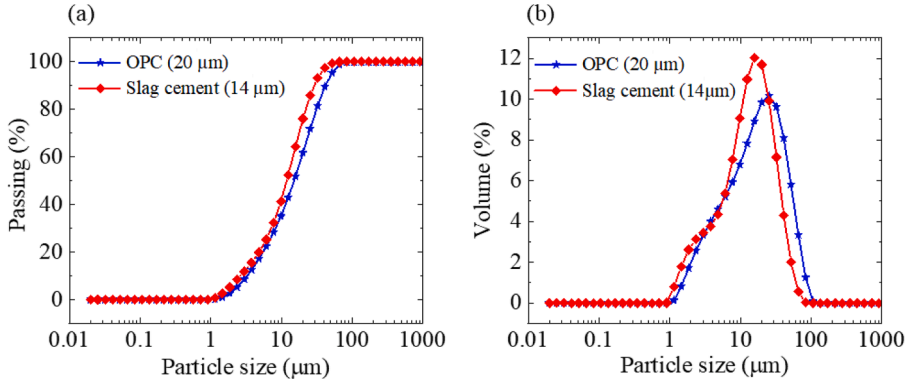

Fig. 1. Particle size distribution of Ordinary Portland Cement (OPC) and Slag cement (SC).

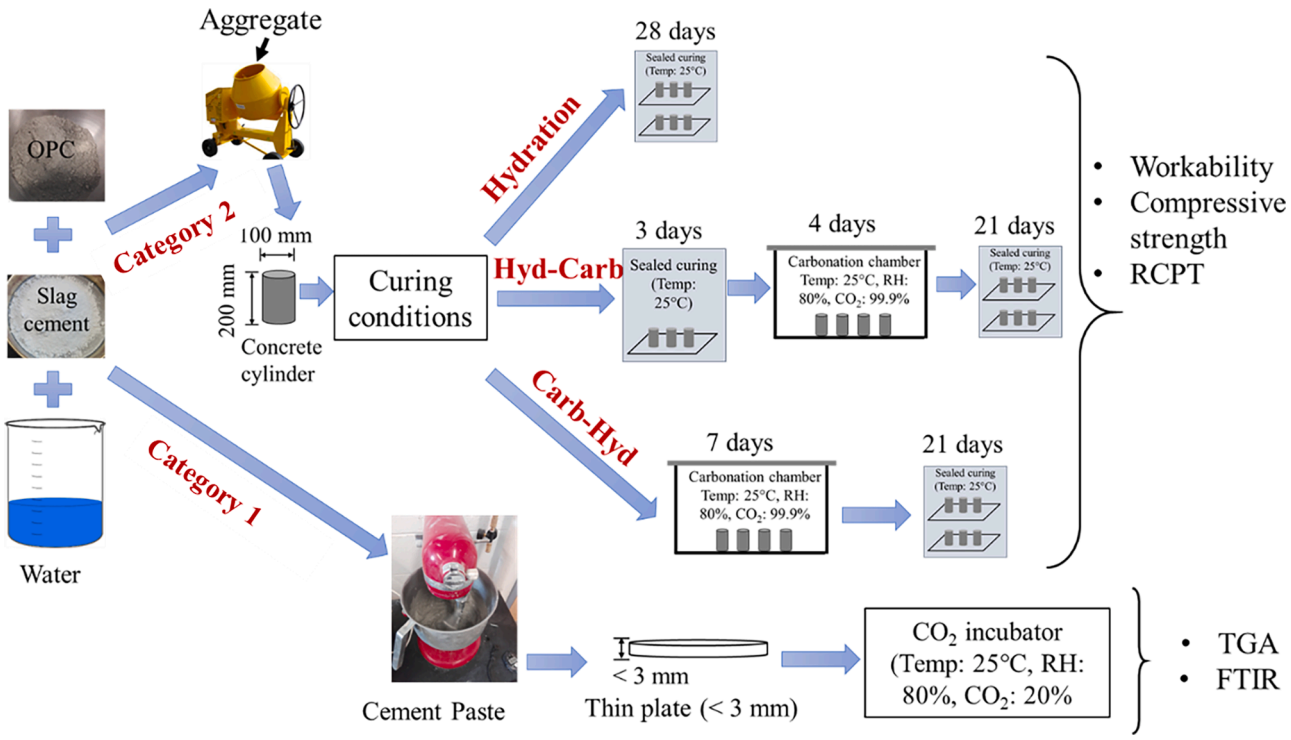

Fig. 2. Schematic presenting the cement paste and concrete sample preparation. Hyd-Carb and Carb-Hyd present 'hydration followed by carbonation' and 'carbonation followed by hydration' curing conditions.

were performed with freshly mixed concrete using ASTM C143 [38].

2.3. Curing condition

Carbonation curing was adopted for the first category of samples (thin paste). After mixing (w/b ratio of 0.4), the paste was spread over a plate with a thickness and diameter of less than 3 mm and 10 mm, respectively, and kept in the 'V.W.R. Air Jacket CO_2 Incubators' for carbonation curing. A temperature of 25 °C, relative humidity (RH) of 80 %, and CO_2 concentration of 20 % were maintained inside the carbonation chamber. Any possible compaction was also avoided in order to eliminate the effect of CO_2 diffusion across the sample. Carbonation curing was performed until 300 h. Small portion of the samples were collected for microstructural analysis at regular intervals (such as 0.5, 3, 6, 10, 24, 72, 145, 200, 300 h). It was assumed that carbonation was not hampered during the sample collection process as relative humidity, temperature, and CO_2 concentration remained constant inside the carbonation chamber.

In the second category of samples, three different curing conditions were used, including hydration curing, hydration-carbonation (Hyd-Carb) curing, and carbonation-hydration (Carb-Hyd) curing, as shown in Fig. 2. Cylinder samples were kept in sealed condition for 28 days in the hydration curing condition. In the hydration-carbonation curing condition, the cylinder samples were kept in sealed condition for 3 days and afterward kept in an unsealed condition in a customized carbonation chamber (Fig. 3) for carbonation curing for four days at 99.9 % CO_2 concentration, then returned to the sealed condition for 21 days. For the carbonation-hydration curing condition, cylinder samples were stored in the unsealed condition in a customized carbonation chamber (at 25 °C, 80 %, RH, and 99 % of the CO_2 was purged) for seven days, and then kept in sealed condition in a moist curing room for 21 days. A reduced CO_2 concentration was used for the first category of samples, compared to the second category, to ensure that the carbonation reaction will be slow enough to monitor microscopic phase formation with time effectively.

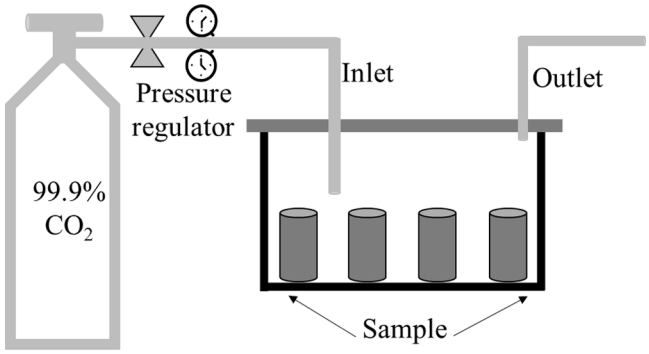

Fig. 3. Customized carbonation setup.

2.4. Test methods

2.4.1. Thermogravimetric analysis (TGA)

The commercially available TGA 550 TA instrument was used in this study. Thin carbonated plate samples (category 1) were used for this test. The thin carbonated sample was first ground using a mortar pestle. Approximately 35 ~ 40 mg of ground powder sample was loaded into a platinum pan and kept in an isothermal condition at around 25 °C for 5 min. Afterward, the temperature of the TGA chamber was increased to 980 °C with a ramp of 15 °C per minute. N_2 gas was purged in the entire process. Initially, three replicate samples were tested through TGA for a few batches to validate any carbonation deviation across samples. The test result deviations were less than 2 % by weight of total carbonated samples. Due to the low deviation, TGA was performed only with one sample for the remainder of the batches. The following decomposition temperatures were used to analyze TGA data in this current study. During the heating process, chemically bound water decomposes from 100~600 °C [36,39,40]. $Ca(OH)_2$ decomposes to CaO and H_2O at around 450 °C [36,39]. $CaCO_3$ decomposes to CaO and CO_2 at 600~800 °C [36,39]. The amount of CaO content in the paste was

calculated from the summation of CaO from $Ca(OH)_2$ and from $CaCO_3$.

2.4.2. Fourier transform infrared spectroscopy (FTIR)

Thin carbonated plate samples (category 1) were ground for this measurement. The commercially available Nicolet iS50 FTIR from Thermo Scientific was used for this test. The spectra were collected using the Attenuated Total Reflection (ATR) mode with 4 cm^{-1} resolution and 32 scans per sample.

2.4.3. Compressive strength test

The compressive strength of the concrete cylinders (sample category 2) was measured using ASTM C39/C39M after 3 days, 7 days, and 28 days of curing [41]. A loading rate of 1780~2670 N/s was used during the compressive strength test. The average compressive strength of the four cylinders was used for each test data presented in this study.

2.4.4. Rapid chloride penetration test (RCPT)

To perform the rapid chloride penetration test, the ASTM C1202 standard test method was followed [42]. The diameter and thickness of the samples were 100 mm and 50 mm, respectively. First, samples of corresponding curing conditions were collected from the core of the cylinder specimens (category 2) following the ASTM C42 standard [43]. Coring was done with a drilling rig equipped with a diamond dressed core bit so that the microstructure would be undisturbed. Once the specimen was ready, it went through the conditioning process as per the standard before starting the test. A commercially available device called Giatec-Perma was used to conduct the rapid chloride penetration test. The test specimen was placed between two cells containing 3 % NaCl solution and 0.3 N NaOH solution.

Upon completion of the 6-hour test, the specimens were removed from the test setup, split in the middle, and then an $AgNO_3$ solution was sprayed on the wet samples after cutting them. This helped to form a white AgCl layer which indicated the chloride penetration into the system [44]. The thickness of the AgCl layer was measured for further analysis, in which the correlation between the chloride penetration depth and the durability of the supplementary cementitious materials was investigated. For determining the chloride ion penetration depth, at least four measurements were taken from each half (Fig. 4).

2.5. Life cycle analysis

2.5.1. Life cycle inventory

The quantity of sand, gravel, and water in the proportion of the binder needed to achieve 1 MPa of compressive strength was calculated, and the results are shown in Table 1. The impact caused by these materials is analyzed separately and combined to achieve the ultimate impact of carbonated and non-carbonated concrete mixes. The binder used per m^3 of concrete was 400 kg/m^3 for all the mixes. For the carbonated samples, sequestered carbon dioxide (CO_2) content was calculated using the TGA plot and subtracted from the global warming potential (GWP) which was obtained from the analysis.

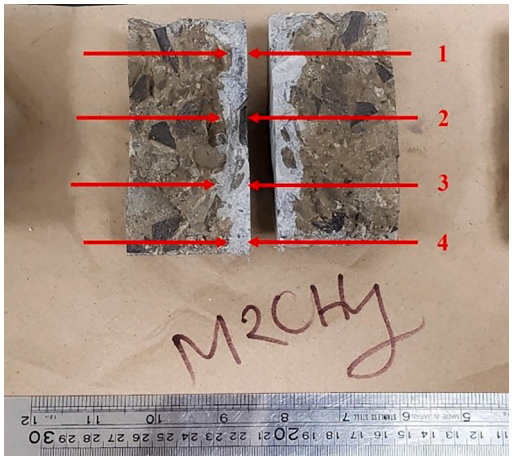

Fig. 4. Measurements of chloride penetration depth.

Table 1
Materials needed to achieve 1 MPa of compressive strength per m^3 of mortar.

Slag content (%)	28 days Compressive strength (MPa)	Cementitious Binder (kg/MPa)	Sand (kg/MPa)	Gravel (kg/MPa)	Water (kg/MPa)
0	40	10.00	17.95	29.30	4.00
45	47	8.51	15.28	24.94	3.40
65	40	10.00	17.95	29.30	4.00
80	32.5	12.31	22.09	36.06	4.92
100	15	26.67	47.87	78.13	10.67

Ecoinvent 3-allocation, cut off by the classification-unit dataset of Sima Pro software, was used as the reference for the life cycle assessment. Table 2 includes the dataset chosen from the Ecoinvent 3 database for each material.

2.5.2. Impact assessment methods

Different impact assessment methods fix the normalization and characterization factors and impact assessment categories. Tool for the Reduction and Assessment of Chemical and other environmental Impacts (T.R.A.C.I.) impact assessment method was employed in this study. This method helps in processing the United States based life cycle analysis. The impact categories presented in this study are Ozone depletion (kg CFC-11 eq), Global warming (kg CO_2 eq), Smog (kg O_3 eq), Acidification (kg SO_2 eq), Eutrophication (kg N eq), Carcinogenic (CTUh), Non carcinogenic (CTUh), Respiratory effects (kg PM2.5 eq), Ecotoxicity (CTUe) and Fossil fuel depletion (M.J. surplus). The US EPA considers environmental impacts with 100-year time horizons [45].

3. Results and discussions

3.1. Microscopic phases analysis

Microscopic phase analysis was performed on the paste samples (category 1) using thermogravimetric analysis (TGA). A typical example of TGA and derivative of thermogravimetry (D.T.G.) plots for 300 h of carbonated OPC-SC samples is shown in Fig. 5. The decomposition temperatures of calcium silicate hydrate (C—S—H), ettringite (AFt), $Ca(OH)_2$, $CaCO_3$ are labeled based on previous studies [36,39,40,46]. The weight loss observed at approximately 50 °C can be attributed to the decomposition of monosulfate and the C—S—H (calcium-silicate-hydrate) gel [36,47–49]. Meanwhile, the weight loss occurring around 100 °C is primarily associated with the decomposition of C—S—H and AFt (ettringite). Further thermal analysis reveals that $Ca(OH)_2$ decomposes around 450 °C, while $CaCO_3$ (calcite) exhibits decomposition in the temperature range of 650 to 800 °C [9,23,24,40,50–52].

All the TGA results were used to quantify the amounts of chemically

Table 2
Dataset used from Ecoinvent 3.

Input	Dataset
Ordinary Portland Cement (OPC)	Cement, Portland (RoW)| market for | Cut-off, U
Slag	Cement, blast furnace slag 70–100 %, non-US {U.S.}| market for cement, blast furnace slag 70–100 %, U.S. only | Cut-off, U
Gravel	Gravel, crushed {RoW}| market for gravel, crushed | Cut-off, U
Water	Water, deionised, from tap water, at user (RoW)| market for water, deionised, from tap water, at user | Cut-off, U
Sand	Sand (GLO)| market for | Cut-off, U

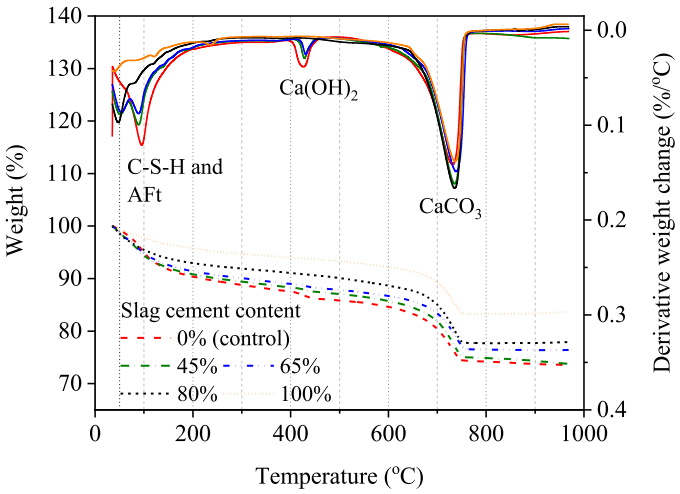

Fig. 5. Typical thermogravimetric plots of paste samples (after 300 h of carbonation) showing different phases.

bound water, $Ca(OH)_2$, and $CaCO_3$ formed in the paste for different SC contents. Fig. 6(b) shows the $Ca(OH)_2$ contents with carbonation duration for different SC contents. All the batches showed a drop in $Ca(OH)_2$ amounts after 6 h of carbonation, followed by an increasing peak at around 24 h of carbonation. From 72 h to 300 h of carbonation, there was no significant change in $Ca(OH)_2$. Chemically bound water content, as given in Fig. 6(a), showed the same trend as $Ca(OH)_2$. It can also be observed that, after 300 h of carbonation curing, the control batch (100 % OPC) contained 9.3 % of chemically bound water. In contrast, the batches containing 45 % and 65 % SC had 8.4 % and 8 % chemically bound water, respectively. The control batch had 6 % $Ca(OH)_2$, while the 45 % and 65 % SC batches had 3.3 % and 3 % $Ca(OH)_2$ content, respectively. The relatively high amounts of $Ca(OH)_2$ and chemically bound water contents in the control batch were expected due to the hydraulic nature of OPC.

The $CaCO_3$ contents in the paste batches are shown in Fig. 6(c). In general, the $CaCO_3$ content was observed to increase with carbonation duration. However, there was a drop in $CaCO_3$ content at around 24 h of carbonation for all the batches, which was reverse of $Ca(OH)_2$ and chemically bound water. So, in this time frame, the hydration reaction accelerated and dominated compared to the carbonation reaction. After 300 h of carbonation the 0 %, 45 %, 65 %, 80 % and 100 % SC batches had 23 %, 24 %, 23 %, 24 %, and 20 % $CaCO_3$ content, respectively. Another important finding from this section is that after 24 h of carbonation, there was an abundance of $Ca(OH)_2$ in the hydraulic and semi-hydraulic systems. After 72 h of carbonation, there was an abundance of $CaCO_3$ content. So at least 72 h of carbonation is required for a higher amount of $CaCO_3$ content than $Ca(OH)_2$ content. It is important to note that even after a longer duration of carbonation, in batches with less than 80 % SC content, complete carbonation of $Ca(OH)_2$ was not achieved. This was attributed to the pore blockage of the system that may have prevented further diffusion of CO_2 into the paste matrix. However, uncarbonated $Ca(OH)_2$ also indicates that these systems are likely to have an alkaline environment. Paste batches containing more than 80 % SC did not have any $Ca(OH)_2$ remaining in the matrix after 300 h of carbonation. Fig. 6(d) shows the total CaO content present in the paste samples in the form of $Ca(OH)_2$ and $CaCO_3$. Since this CaO came out from the unreacted OPC and slag, the total CaO content was used as an indicator of the degree of reaction. As observed from this

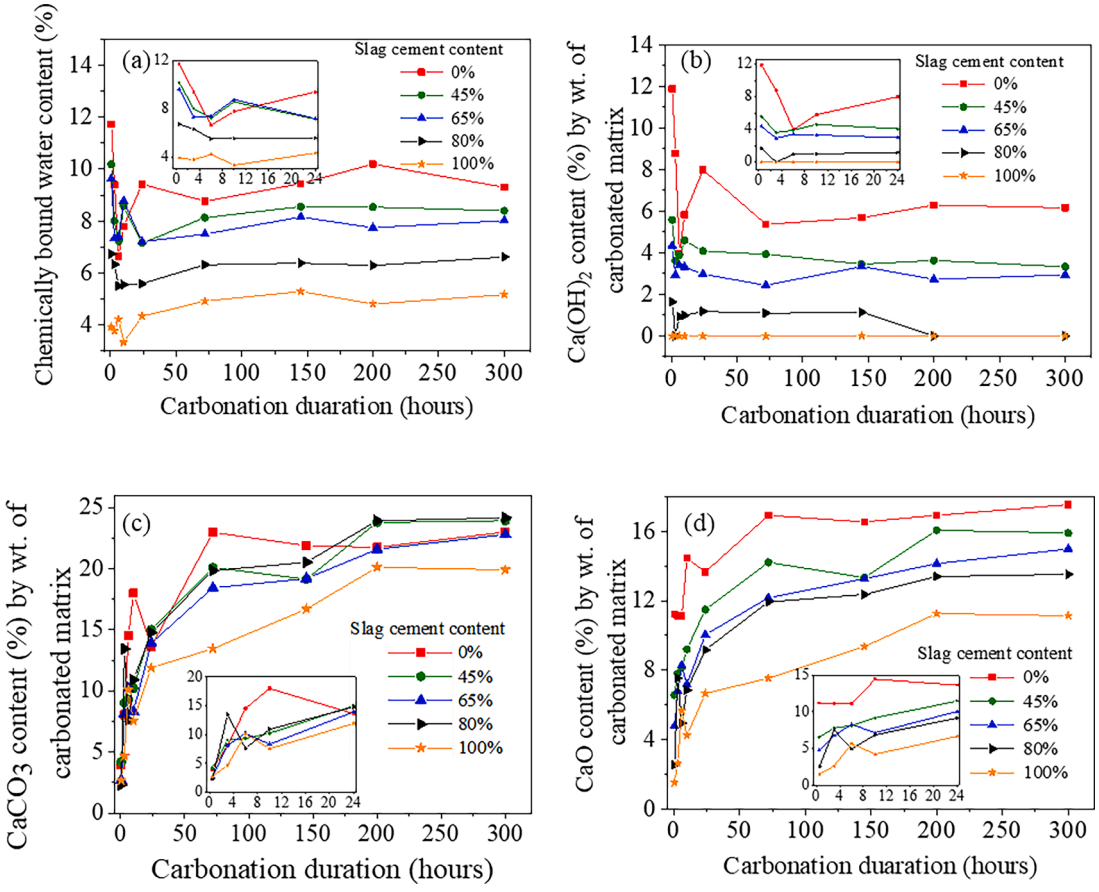

Fig. 6. Thermogravimetric analysis (TGA) results, (a) chemically bound water content, (b) $Ca(OH)_2$ content, (c) $CaCO_3$ content, and (d) CaO content with carbonation duration. The inset portion of each figure is the enlarged image showing the variations within 0 to 24 h.

figure, the control (0 % SC) and 100 % SC batches had the highest and lowest amounts of CaO contents, respectively.

Fig. 7 shows the theoretical and experimental values of $CaCO_3$ content. Theoretical values were calculated based on the following Eq. (1). It can be observed from the figure that the inclusion of OPC and SC together results in $CaCO_3$ contents that are higher than the theoretical values. Specifically, after 300 h of carbonation, all the combinations of SC and OPC resulted in $CaCO_3$ contents that were higher than the expected theoretical value. This further indicates that the carbonation reaction is more efficient for the OPC and SC combinations compared to the OPC- or SC-only batches. Based on this observation, concrete samples that were used for mechanical and durability testing were carbonated for a minimum of 72 h.

$$\textit{Theoretical } CaCO_3 \textit{ content } (\%) = \textit{Slag cement content in the mix} \times CaCO_3 \textit{ content } (\%) \textit{in } 100\% \textit{ slag cement content batch} + \textit{OPC content in the mix} \times CaCO_3 \textit{ conetent in } 100\% \textit{ OPC content batch} \quad (1)$$

3.2. Carbonation reaction rates

Based on the previous study [17,53], the carbonation process of OPC-SC was divided into two distinct stages. Stage-1 represents a 'phase boundary controlled' reaction where reactions take place at the reactive phase boundary. A rapid rate of carbonation can be expected during this stage. Stage-2 represents the 'products layer diffusion controlled' reaction. Ionic diffusion through the product layers formed in stage-1 controlled the reaction in this stage. The reaction rate in stage-2 was slower than the stage-1 reaction rate.

The degree of carbonation was calculated based on Eq. (2). The reaction rate constant was determined by fitting the degree of carbonation in the generalized Eq. (3), shown in Fig. 8(a). A similar procedure was followed for calculating the reaction rate constant for Ca-based materials by other researchers [53,54].

$$\textit{Degree of carbonation, } \alpha = \frac{\textit{Amount of } CaCO_3 \textit{ (weight \%) at time } ``t"}{\textit{Maximum amount of } CaCO_3 \textit{ (weight \%) formed}} \quad (2)$$

$$\left[1-(1-\alpha)^{\frac{1}{3}}\right]^{n} = kt \quad (3)$$

Here, `k' denoted the reaction rate constant, `t' denoted the carbonation duration, and `n' was the factor that indicates reaction controlling steps. The exact reaction rate constant depends on several experimental variables, that's why the apparent value of the reaction rate constant was used here. In Eq. (3), $n = 1$ represents the contracting volume equation [17,55]. This represents the geometric contractions mechanism for stage-1 carbonation. This mechanism consists of rapid and dense nucleation and rapid surface growth. The reaction front moves from the surface to all particles. For $n = 2$ of Eq. (3) represents the Jander equation, which represents a reaction controlled by diffusion through product layers. This represents the stage-2 reaction mechanism in this study.

$$\ln\left[1-(1-\alpha)^{\frac{1}{3}}\right] = \frac{1}{n}\ln(t) + \frac{1}{n}\ln(k) \quad (4)$$

The logarithm form of Eq. (3) is shown in Eq. (4). Using the linear relationship of Eq. (4), the reaction constants were determined for both stages. Fig. 8(a) shows the fitted plot of the degree of carbonation, and Fig. 8(b) shows the reaction rate constant. For ideal cases, the slope of the fitted plots of stage-1 and stage-2 were 1.0 and 0.5, respectively [53]. However, from experimental data, the slopes of stage-1 and stage-2 were between 0.4~0.6 and 0.2~0.4, respectively. The reasons for the deviation of those values from the ideal cases are explained elsewhere [53].

The reaction constant k_1 was larger than k_2 due to the rapid carbonation rate during stage-1. The k_1 value was highest for the 0 % SC batch and lowest for 100 % SC batch. This variation was due to the initial higher reactivity of OPC and slow reactivity of SC. In the case of the k_2 value, the 45 % SC batch has a higher value than the other batches. That is why this batch gave a high $CaCO_3$ content after 300 h of carbonation.

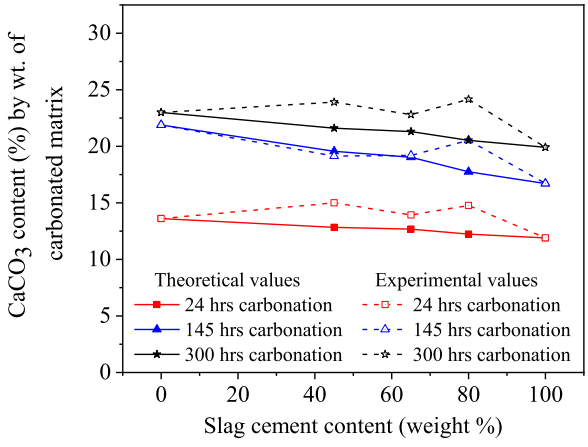

Fig. 7. Comparison of $CaCO_3$ with theoretical and experimental values.

3.3. Polymerization of the calcium-silica gel product

The peaks in the wavenumber, ranging from 800 cm^{-1} to 1200 cm^{-1}, were due to the Si—O bond's asymmetric and stretching vibration ($\nu 3$) [56,57]. The exact location of these peaks depends on the Ca/Si ratio [56]. The band of calcium silicate hydrate (C—S—H) gel can be observed at around 950 cm^{-1}, and this was due to the Si—O stretching vibration (ν_3) of the Q^2 tetrahedron [13,28,56,58]. Hydrated OPC primarily contains a C—S—H gel consisting of Q^1 and Q^2 tetrahedron in ^{29}Si N.M.R. [54]. Details of this Q^0 to Q^4 arrangements of silica tetrahedra can be found elsewhere [54].

The absorbance band at and below 800 cm^{-1} was due to out-of-plane and in-plane skeletal (ν_4) vibration of Si—O [56] and was not studied here. The band range from 1400 cm^{-1} to 1500 cm^{-1} was due to asymmetric stretching (ν_3) of CO_3^{2-} and the 872 cm^{-1} band was due to out-of-plane bending vibration (ν_2) of CO_3^{2-} [57,59]. The bending peak vibration at around 1639 cm^{-1} was due to the $Ca(OH)_2$ and chemically bound water [57,60]. This peak was previously reported to shift a higher wavenumber due to carbonation [57].

This study focused on analyzing the peaks ranging from 800 to 1800 cm^{-1} to study the calcium-silica gel polymerization. The shift of the 950 cm^{-1} band to a higher wavenumber was due to the increasing degree of silica gel polymerization and the higher bond strength of Si—O [56,57,61,62]. Fig. 9 shows the FTIR spectra for different carbonation durations and different SC contents. The out-of-plane vibration (ν_2) of CO_3^{2-} at 872 cm^{-1} was due to the calcite [57,59]. The calcite peak increased in intensity with carbonation duration [Fig. 9(a–d)], indicating higher amounts of calcite formation. The 950 cm^{-1} peak, due to the Si—O bond in the C—S—H gel, was found after 0.5 h of carbonation, as shown in Fig. 9(a) [63]. This peak at 950 cm^{-1} decreased and shifted to higher

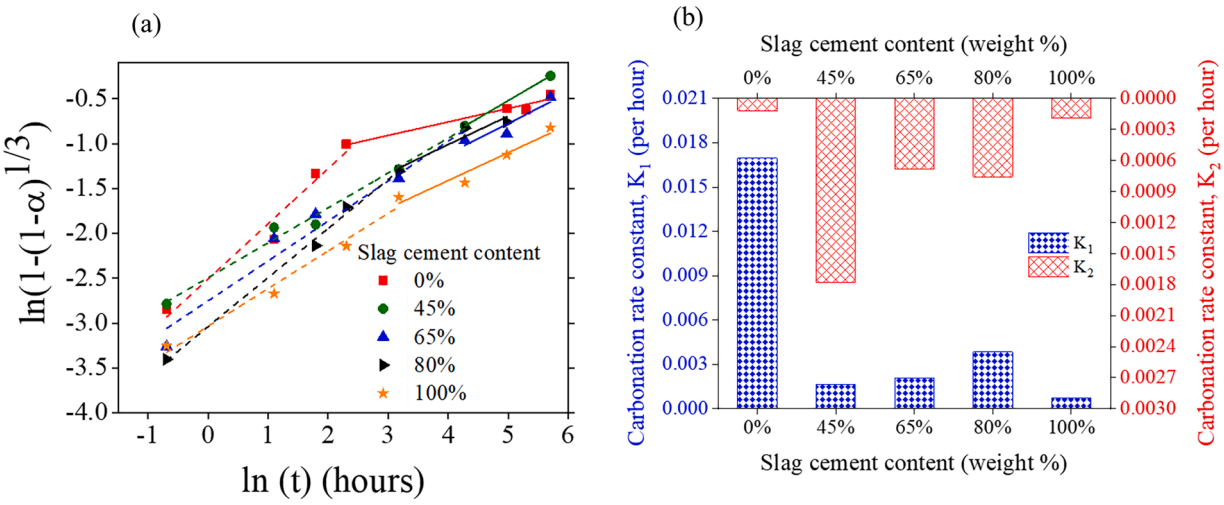

Fig. 8. (a) Theoretical kinetics model with data fitting (dashed lines represent stage-1 reaction, solid lines represent stage-2 reaction), (b) reactions rate constants (per hour). The left y-axis represents K_1, and the right y-axis represents K_2.

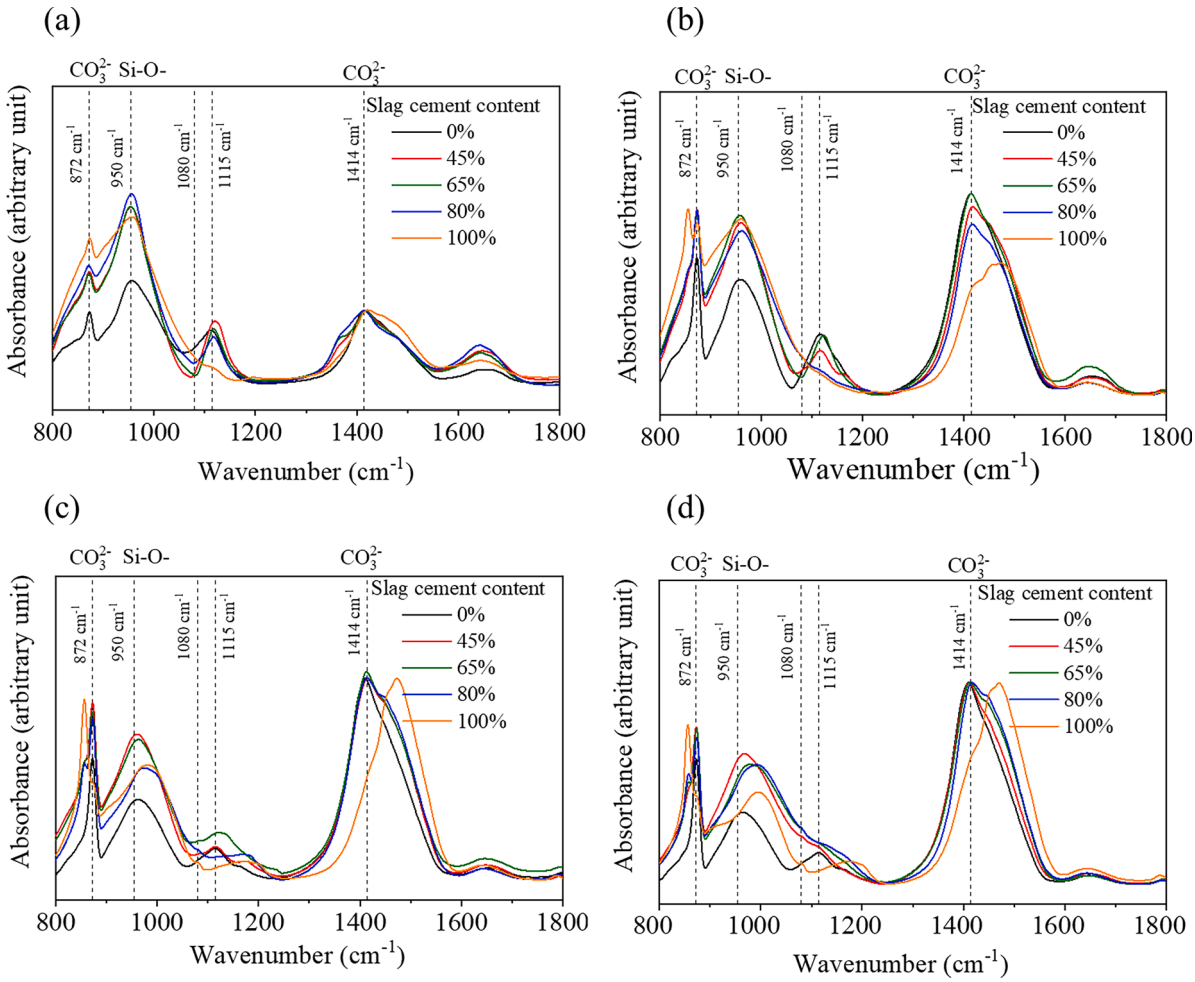

Fig. 9. Normalized FTIR spectra of the OPC-SC carbonated paste after (a) 0.5 h, (b) 24 h, (c) 145 h, and (d) 300 h of carbonation.

wavenumbers with increasing carbonation and also with increasing SC content. This is due to silica gel polymerization and the formation of Ca-modified silica gel from the C—S—H gel during the carbonation. Due to the silica gel polymerization, additional peaks were observed to form around 1080 and 1115 cm^{-1}, as shown in Fig. 9(c, d). These peaks were assigned to Q^3 and Q^4 sites for wavenumbers of around 1089 cm^{-1} and 1135 cm^{-1}, respectively. The formation of these peaks indicates the decalcification of C—S—H gel and the presence of higher amounts of silica gel [64]. The decalcification of C—S—H and subsequent polymerization of silica gel during the carbonation of the OPC-SC blends were observed by the reduced intensity of Q^2 and increased intensity of Q^3 and Q^4 peaks (Fig. 9). The sharp ν_3 peak at around 1414 cm^{-1} was

due to calcite formation [65], and the overlapped stretching vibrational peak at around 1490 cm^{-1} was due to the vaterite formation [60,66]. As observed from Fig. 9, an increased amount of SC resulted in higher amounts of vaterite formation during carbonation.

The FTIR spectra were deconvoluted using commercially available software (OriginPro 2017) to quantify the peaks due to the C—S—H gel and Ca-modified silica gel. The FTIR spectra of the carbonated samples were subjected to deconvolution to accurately determine the wavenumber associated with the ν_3 vibration of the Si—O bond. This analysis was conducted following the methodology established in a prior study [56,64,67,68]. The deconvolution results of the various SC content batches carbonated for 300 h are shown in Fig. 10. The Si—O bond shifted to 968 cm^{-1} and another peak at 1114 cm^{-1} was formed due to the silica gel polymerization of the 0 % SC batch, as shown in Fig. 10(a). For the 45 %, 65 %, 80 % and 100 % SC batches, the Si—O bonds shifted to 966, 979, 991, and 993 cm^{-1}, respectively. This indicates that with increasing SC content, the silica polymerization in the calcium-silica gel increased. The Q^3 peaks were at 1064, 1102, 1139, 1167 cm^{-1} for the 45 %, 65 %, 80 %, and 100 % SC batches, respectively, further indicating that the final calcium-silica gel hydration product in SC batches has a higher degree of silica gel polymerization.

The mean wavenumber due to Si—O bond was calculated based on Eq. (5) [56].

$$I_{mean} = \frac{I_i A_i + \ldots + I_N A_N}{A_i + \ldots + A_N}. \quad (5)$$

Here, I_{mean} is the mean wavenumber of Si—O (ν_3) vibration. $I_i \ldots I_N$ are the wavenumbers corresponding to the bands i…N. $A_i \ldots A_N$ represents the area under the bands of $I_i \ldots I_N$. The mean wavenumbers of different SC contents for 300 h of carbonations have been plotted. Fig. 11 shows the variation of wavenumbers corresponding to the Si—O ν_3 vibration bond with different SC contents. The linear fit line shows the gradual shifting of the Si—O bond to higher wavenumbers with increasing SC contents. Average minimum and maximum wavenumber were obtained as 991 cm^{-1} and 1021 cm^{-1}, respectively, although the actual minimum and maximum wavenumber were 964 cm^{-1} and 1139

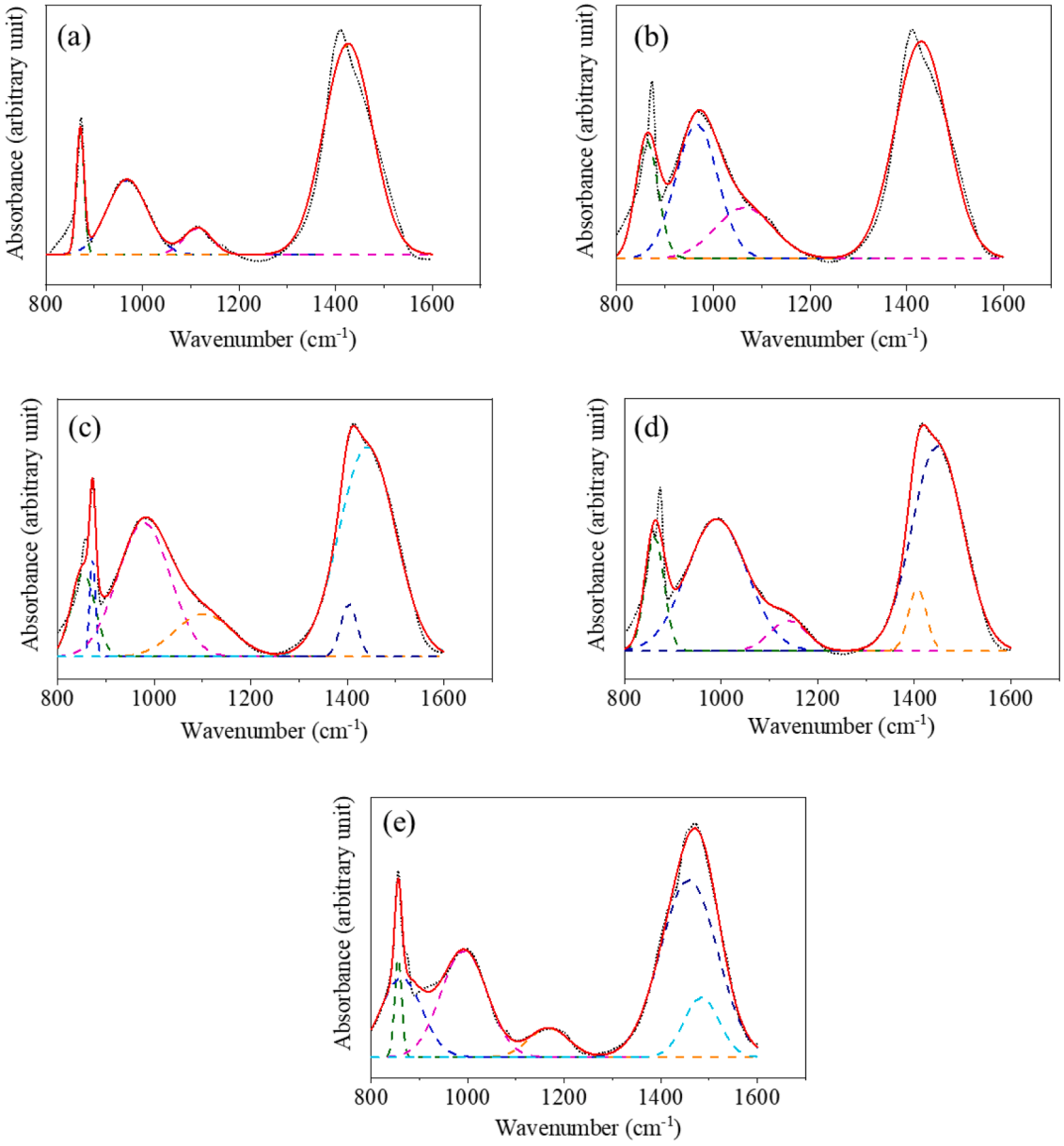

Fig. 10. Deconvolution of FTIR spectra of 300 h of carbonation, (a) 0 % SC content, (b) 45 % SC content, (c) 65 % SC content, (d) 80 % SC content, (e) 100 % SC content. Dotted line, solid line and dashed line represent experimental FTIR spectra, simulated spectra and deconvoluted absorbances bands, respectively.

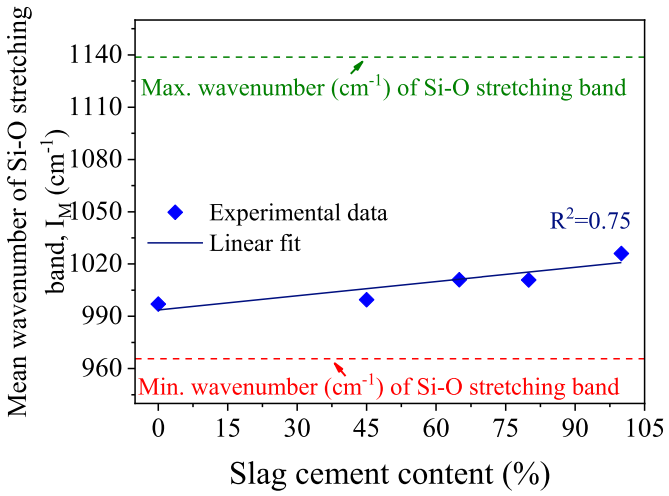

Fig. 11. Mean wavenumber of Si—O stretching band with slag cement content.

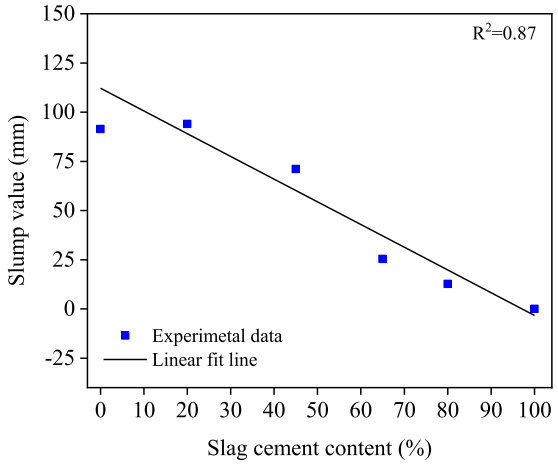

Fig. 12. Concrete workability (i.e., slump) due to the addition of slag cement.

cm^{-1}. This implies a higher number of Q^3 tetrahedron sites in the carbonated matrix.

3.4. Workability

The slump of the freshly made concrete samples is shown in Fig. 12. The slump value of the control batch was measured to be 92 mm. The workability of the 20 % SC batch was increased by 2 % over the control batch. On the other hand, workability decreased by 22 %, 72 %, 86 %, and 100 % for the 45 %, 65 %, 80 %, and 100 % SC batches, respectively. This finding is similar to the previously reported data [69–72]. Due to the vitreous appearance of SC, when a small amount of OPC was replaced by SC, the workability increased by improving the dispersion of the particle [73]. On the contrary, since SC has a smaller particle size than OPC, the more significant amount (more than 45 %) of OPC replacement by SC reduced its workability due to the increase in surface area and decrease in the inter-particle distance [71]. The angular shape of the SC particle is another possible reason for decreased workability [70].

3.5. Compressive strength

The results of the cylinder compressive strength of the different curing conditions are shown in Fig. 13. The compressive strength of concrete samples after 3 days, 7 days and 28 days hydration curing are given in Fig. 13(a). Concrete batches containing 45 %, 65 %, 80 %, and 100 % of slag cement provided compressive strengths that are 19 %, 13 %, 35 %, and 82 % lower, respectively, compared to the control batch. The 20 % SC batch achieved the same compressive strength as the control batch (100 % OPC) after 3 days of hydration curing. After 7 days of hydration curing, the 45 % SC batch showed the highest compressive strength, 5 % higher than the control batch. The other batches, i.e., 20 %, 65 %, 80 %, and 100 % SC batches showed a decrease in compressive strength of 5 %, 6 %, 32 %, and 80 %, respectively. After 28 days of hydration curing, the 45 % SC batch showed a 16 % increase in compressive strength, and the 20 % and 65 % SC batches were the same as the control batch. The 80 % and 100 % SC batches have reduced the compressive strength by 21 % and 63 %, respectively. Based on these results, it can be concluded that 45 % of OPC can be replaced with SC cement without any detrimental effect on the mechanical performance in the case of hydration curing.

Fig. 13(b) shows the compressive strengths of concrete cylinders cured in the hydration-carbonation conditions. The results of the first three days of compressive strength were the same as for the hydration curing. After 7 days, the 20 %, 45 %, and 65 % SC batches showed a 10 %, 6 %, and 12 % increase in compressive strength, respectively. The 80 % and 100 % SC batches showed 20 % and 74 % decrease in compressive strength compared to the control batch. After 28 days, the 80 %, 20 %, 45 % and 65 % SC batches showed 9 %, 12 %, 19 %, and 30 % higher compressive strength, respectively. The 80 % and 100 % SC batches showed a 15 % and 68 % decrease in compressive strength compared to the control batch. Therefore, in the case of the hydration-carbonation curing condition, the optimum SC content is 65 %.

Fig. 13(c) shows the compressive strengths of concrete cylinders cured in carbonation-hydration conditions. After 3 days of curing, the 20 % SC batch showed a 5 % increase in compressive strength. The 45 %, 65 %, 80 % and 100 % SC batches showed a 12 %, 9 %, 28 % and 81 % decrease in compressive strength, respectively, compared to the control batch. After 7 days of curing, the concrete batches with 0 %, 20 %, 45 % and 65 % SC provided a 4 %, 6 %, 15 %, 14 % increase in compressive strength, respectively. The 80 % and 100 % SC batches provided 22 % and 76 % less compressive strength, respectively. After 28 days, the 0 %, 20 %, 45 %, and 65 % SC batches provided a 12 %, 17 %, 16 %, and 10 % increase in compressive strength, respectively, compared to the control batch (hydration-cured 100 % OPC batch). The 80 % and 100 % SC batches provided 20 % and 70 % less compressive strength, respectively. Therefore, in the case of the carbonation-hydration curing condition, the optimum SC content is 45 %.

Fig. 13(d)–(f) show the percentage changes in compressive strengths of the concrete samples with respect to the control batch due to different SC contents, curing conditions, and curing durations. The concrete batch with 100 % OPC subjected to hydration only was considered as the control batch. Fig. 13(d) shows that after 3 days of curing, almost all the batches containing SC showed a lower compressive strength than the control batch. This is expected due to the slow reactivity of slag. Nonetheless, the concrete batch containing 20 % SC shows slightly higher compressive strength compared to the control batch when subjected to carbonation curing. All the carbonation-cured batches also showed higher strength compared to the batches subjected to hydration only. After 7 days [Fig. 13(e)], incorporating carbonation curing resulted in a higher compressive strength than the control batch. At this stage, the 'carbonation-hydration' curing condition resulted in higher strengths compared to the 'hydration-carbonation' curing condition. Further, it is evident from the plot that both 'hydration-carbonation' or 'carbonation-hydration' curing conditions will allow up to 65 % cement to be replaced with SC without degrading the strength. Based on the 28 days strength results [Fig. 13(f)], incorporation of carbonation curing still provides superior strength compared to the control batch, even after replacing up to 65 % of OPC with SC. For both the 7-day and the 28-day compressive strength results, incorporation of carbonation resulted in a higher increase in strength, up to 65 % SC content, compared to the batch with 0 % SC. Therefore, the efficiency of carbonation curing is

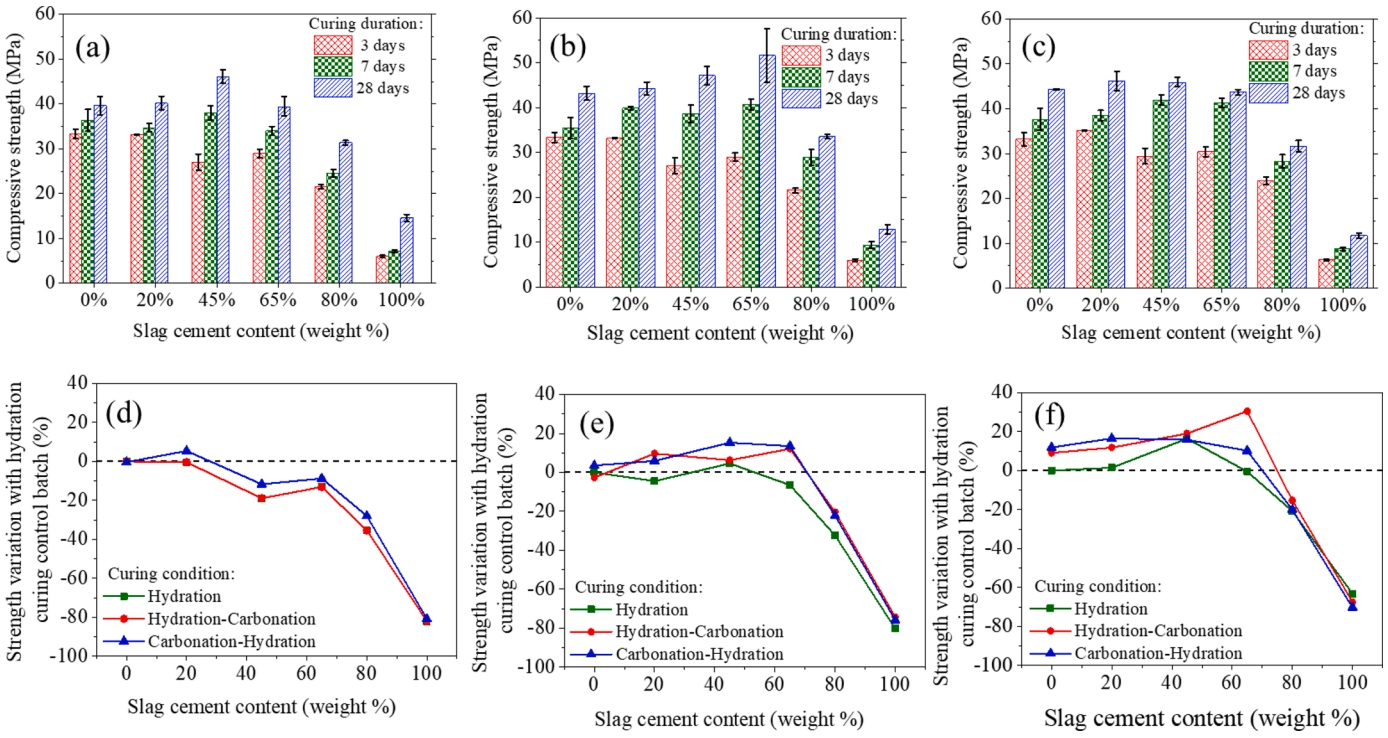

Fig. 13. Cylinder compressive strength test of curing condition (a) hydration, (b) hydration-carbonation, (c) carbonation hydration. Strength variation with respect to control batch of hydration curing for curing duration of (d) 3 days, (e) 7 days, and (f) 28 days.

enhanced when a higher amount (up to 65 %) of SC is used in the concrete mixture. However, as observed from the compressive strength test results, the strength of the 0 % slag was not the highest. Although 0 % SC showed higher reactivity, as discussed in Section 3.1. This indicates that the extent of the reaction and the types of reaction products play a crucial role in the mechanical performance of carbonated matrixes. A balance of $Ca(OH)_2$ and $CaCO_3$ results in high strength based on the results.

3.5.1. *Statistical (t-test) analysis of compressive strengths*

The 'Two-sample t-test' statistical technique was used to evaluate the significant effect of slag cement content and curing conditions on cylinder compressive strength. The compressive strength was compared with respect to the hydration-cured control batch (0 % SC content). The test was conduct at a confidence level of 95 %. Statistical *p*-values less than 0.05 implied a statistically significant difference between the two groups of samples and vice versa.

The results of the *t*-test analysis are given in Table 3. There was no substantial increase in compressive strength after 3 days and 7 days of hydration curing due to the addition of slag cement. On the other hand, after 28 days, the sample with 45 % SC content showed significantly higher compressive strength than the control batch under the hydration curing condition.

Compared to the effects of hydration curing, hydration-carbonation curing provided statistically enhanced compressive strength. A significant increase in compressive strength was observed with an increase in SC content and curing duration, although 45 % SC content had not provided significantly higher compressive strength at 7 days yet. There was not significant effect of carbonation curing on 0 % SC content batch until 7 days.

There was no significant increase in compressive strength of up to 20 % of SC content and up to 7 days of curing duration for the carbonation-hydration curing condition. Significant compressive strength was achieved for more than 20 % of SC content. The above discussion concludes that statistically significant strength can be achieved with increasing SC content and incorporating carbonation curing conditions with a longer curing duration.

3.6. *Testing of concrete resistivity against chloride ions*

For cement concrete systems, the durability of concrete plays a significant role in controlling the service life [74]. Importantly, the durability of concrete mainly depends on the capacity to resist fluid penetration into the microstructure of the concrete, which is called permeability [74]. Concrete permeability is closely related to the

Table 3
Statistical (*t*-test) analysis results (*p*-values) of concrete compressive strength.

Slag cement content (wt.%)	Curing conditions								
	Hydration			Hydration-carbonation			Carbonation-hydration		
	3 days	7days	28 days	3 days	7days	28 days	3 days	7days	28 days
0	–	–	–	**–**	**0.31**	0.04	**0.45**	**0.26**	0.03
20	**0.42**	**0.14**	**0.35**	**0.42**	0.03	0.02	**0.05**	**0.09**	0.009
45	0.0054	**0.15**	0.0072	0.0054	**0.11**	0.006	0.019	0.007	0.01
65	0.003	**0.075**	**0.45**	0.003	0.015	0.03	0.016	0.01	0.03
80	0.0002	0.0006	0.009	0.0002	0.003	0.017	0.0002	0.002	0.004
100	0.0001	0.000007	0.0005	0.0001	0.00003	0.0002	0.0002	0.00007	0.0005

**Note:* Bold fonts represent (*p*-values>0.05) no significant variation in strength compared to the control batch.

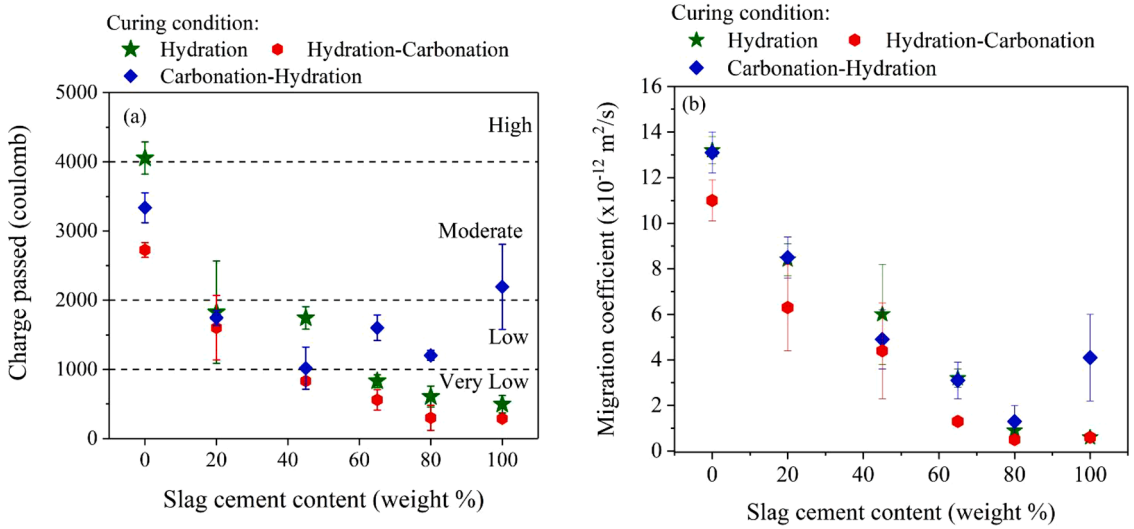

Fig. 14. (a) Rapid chloride permeability test (RCPT) results; (b) Non steady state migration coefficient.

intensity of microcracks at the aggregate-cement paste interface [75]. Therefore, the rapid chloride permeability test (RCPT) test was performed to monitor the effects of carbonation curing on the durability performance of concrete.

From the standard, it is known that there are five categories of chloride ion permeability based on the amount of charge passed. They are: high (>4000C), moderate (2000C–4000C), low (1000C–2000C), very low (100C–1000C) and negligible (<100C). Fig. 14(a) shows the plot of the total charge passed versus the slag cement content. Among the batches, the higher slag content ones had lower total charges passed into their system. Furthermore, in the case of the curing conditions, it was found that the hydration-carbonation batches exhibited the lowest amount of charges among the three curing conditions. These results showed relevance combined with the compressive strength results, for which the hydration-carbonation batches exhibited the highest strength. The more compressive strength indicates a denser matrix in the system, which allows less charge to penetrate. The 0 % SC batch exhibited the least resistance to charge, and it fell under the moderate range. The hydration and carbonation-hydration batches of 20 % and 45 % SC content fell under the low range, whereas the hydration-carbonation batches of the same SC content fell under the very low range. From the previous Section 3.4, the 65 % SC batch showed the highest strength, and here it showed the most resistance to charge passing.

Although taking data from the rapid chloride penetration test at short time intervals (here 30 mins) can erase the temperature effect on the passing charge, this method may not always portray correct assessment of chloride ion permeability because concrete with low resistivity does not necessarily have a high chloride ions diffusivity [76]. Thus, it can be misleading to consider passing charges only to determine chloride ions penetrability in concretes. That is why further investigation was conducted by extending the RCPT test. Once the rapid chloride penetration test ended, the average chloride ion penetration depth was determined, from which chloride ion diffusion due to non-steady state migration were calculated using Eq. (6) [77].

$$D = \frac{0.0239(273+T)*L}{(V-2)*t}\left(X_d - 0.0238\sqrt{\frac{(273+T)*L*X_d}{V-2}}\right) \quad (6)$$

Where D = non-steady-state migration coefficient (x10^{-12} m^2/s),

V = applied voltage (V),

T = average value of initial and final temperatures in the anolyte solution (°C),

L = thickness of the specimen (mm),

X_d = average value of penetration depth (mm), and

t = time (hour).

Fig. 14(b) exhibits the plot of migration coefficients versus slag cement content, where the correlation was observed that the more charge passed, the more chloride ion diffusion in the system. As the penetration depth was taken measuring at four spots due to its non-uniformity, the standard deviation was found to be slightly higher. It was found that for 45 % SC content with the hydration-carbonation curing condition, the diffusion coefficient was 27 % lower than for the hydration-only curing batches. For 65 % SC content, the coefficient for the hydration-carbonation curing was reduced by 60 % compared to the hydration-only batch. Apart from these two superior batches, the other slag cement content batches also had lower diffusion coefficients compared to the hydration-only and carbonation-hydration curing condition batches. The samples with the lowest charge consumption still showed the best resistance to chloride ion diffusion.

3.7. *Environmental impact analysis of the carbonated and non-carbonated concrete mixes*

3.7.1. *Effect of carbonation on global warming potential*

The calculated global warming potential (GWP) caused by both carbonated and non-carbonated concrete mixes is presented in Fig. 15. It is observed that replacing OPC by 45–80 % slag can reduce the global warming potential by 36–39 % in non-carbonated concrete mixes. While GWP reduction was 32–42 % because of the slag replacement in carbonated concrete mixes. However, using 100 % slag as binder

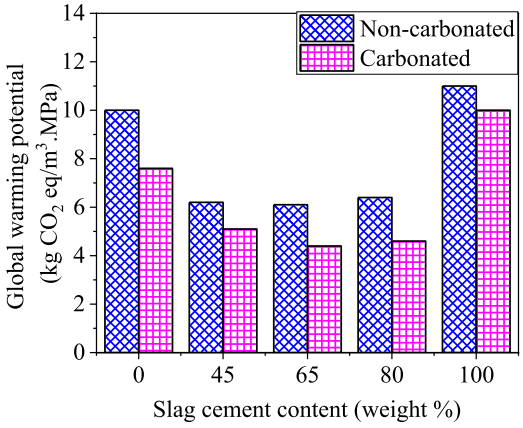

Fig. 15. Global warming potential for different mixes.

provides significantly low compressive strength. Therefore, despite generating less CO_2, the requirement of increasing binder quantity to increase strength eventually increases the global warming potential. Sequestrating CO_2 in concrete mixes causes reduction of GWP by 14–25 % relative to their respective non-carbonated concrete mix. Among the mixes, the carbonated concrete mix with 65 % slag content gives the lowest GWP (4.6 kg CO_2 eq).

3.7.2. Environmental impact caused by the carbonated mortar sample

The impact for each of the environmental categories for carbonated and non-carbonated concrete samples are shown respectively in Fig. 16 (a) and (b). The impact for both type of samples was normalized with respect to the non-carbonated concrete sample with 100 % OPC binder. It is observed that all the environmental categories have high impact values for the mixes with 100 % and 80 % slag content. As discussed above, due to having low compressive strength, increased demand for

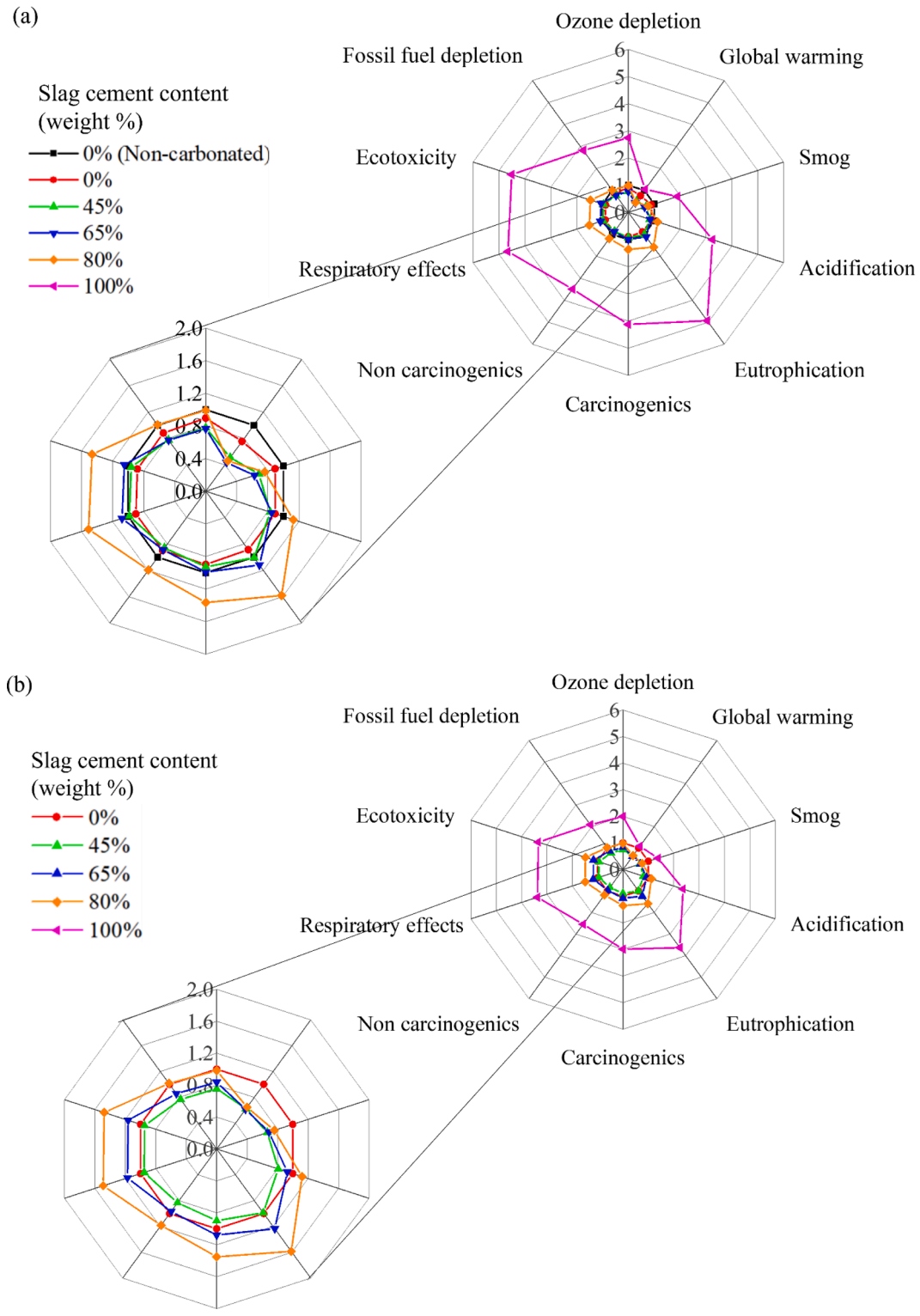

Fig. 16. Normalized impact values for (a) carbonated and (b) non-carbonated concrete mixes. Here, NC: No carbonation, C: Carbonation cured.

binder content has caused this fact. Though, replacing OPC by 45 % slag can help reducing the impacts, the reduction is not significant. Therefore, carbon dioxide was sequestrated into the concrete to improve this condition. CO_2 sequestration has increased the compressive strength, reduced the binder quantity, and contributed to CO_2 storage, thereby reducing the GWP. It is observed that, carbonated concrete sample with 45 % and 65 % slag content has lesser environmental impacts relative to the carbonated and non-carbonated concrete sample with 100 % OPC binder. Moreover, environmental impacts can be reduced just by sequestrating CO_2 without any slag replacement. It is evident from Fig. 16 (b) where carbonated 100 % OPC concrete has less impact relative to non-carbonated 100 % OPC concrete.

The efficiency of CO_2 sequestration in cement pastes when using SC as a OPC substitute hinges on two primary factors. Firstly, it relies on the dissolution rate, quantity, and diffusion of Ca^{2+} originating from both OPC and SC into the pore solution. Secondly, it depends on the rate at which CO_2 dissolves in water and traverses the capillary pore network within the paste. In terms of the former aspect, $Ca(OH)_2$, a byproduct of cement hydration, dissolves readily in the pore solution, leading to rapid carbonation. In as little as 3 days of exposure of CO_2, a significant portion of $Ca(OH)_2$ undergoes carbonation, as confirmed by TGA findings. As Ca^{2+} becomes depleted, it may be liberated from the decomposition of substances like ettringite, $CaCO_3$, C—S—H, and C—A—S—H. Consequently, the diffusion of Ca^{2+} and CO_3^{2-} prompts the formation of calcium-rich carbonates, creating a carbonate layer on the surfaces of SC particles.

4. Conclusions

This article presented a study on the synergy between OPC and SC for carbonation curing. In summary, the following observation can be made based on this study,

I. Concrete cylinder compressive strength was measured in three curing conditions. Among those three curing conditions, the highest compressive strength resulted from 28 days of hydration-carbonation curing, which consisted of 3 days of hydration, 4 days of carbonation, and then the remaining 21 days of hydration. Therefore, accelerated carbonation curing is advantageous when the concrete is allowed to hydrate briefly.
II. TGA results showed that the chemically bound water and Ca $(OH)_2$ content remained the same after 72 h of carbonation up to 300 h of carbonation. The blended batches containing less than 80 % SC were found to have uncarbonated $Ca(OH)_2$ even after long-term (i.e., 300 h) carbonation duration.
III. The actual amount of $CaCO_3$ formed in OPC-SC blended systems was higher than the theoretical value, indicating that the addition of SC improves the carbonation efficiency of the OPC-SC blended system.
IV. The polymerization of calcium-silica gel product formed during the carbonation of OPC-SC blend systems varies depending on the blend ratio. Specifically, increasing SC content increases the silica gel polymerization of the gel.
V. Increasing SC content in the OPC-SC blend was found to result in higher amounts of vaterite compared to the 100 % OPC which only had calcite.
VI. Incorporation of carbonation curing helps achieve higher mechanical performance from OPC-SC blended systems after both 7 days and 28 days curing. An SC content in the range of 45 % to 65 % was found to result in maximum benefit, with a 65 % replacement level resulting in the highest mechanical strength using the hydration-carbonation curing regime.
VII. Among the mixes, the carbonated concrete mix with 65 % slag content gives the lowest GWP (4.6 kg CO_2 eq). It is observed that, the carbonated concrete sample with 45 % and 65 % slag content has lesser (50 to 60 % lower) environmental impacts relative to the carbonated and non-carbonated concrete sample with 100 % OPC binder.

One crucial observation is the superior compressive strength achieved with hydration-carbonation curing, emphasizing the significance of the curing process. The selection of an SC content ranging from 45 % to 65 % is pivotal, as it led to the most substantial mechanical strength and 75 % reduction in the chloride permeability, particularly when exposed to the hydration-carbonation regime. The 65 % OPC replaced by SC and exposed to carbonation curing, provided 20 % higher compressive strength, highlighting the potential of SC to enhance concrete's structural properties.

From an environmental perspective, the incorporation of SC reduced the global warming potential (GWP) by 60 %, demonstrating its eco-friendly attributes. Moreover, the sequestration of carbon dioxide within the concrete matrix led to additional reductions in GWP, aligning with sustainable construction objectives.

This study offers a promising avenue for the concrete industry by combining enhanced mechanical performance and environmental sustainability. The optimal SC content and curing conditions represent a practical strategy for producing high-performance, eco-conscious concrete. Future research should focus on the long-term durability and scalability of these findings, paving the way for widespread adoption in construction practices.

Declaration of Competing Interest

The authors declare that they have no known competing financial interests or personal relationships that could have appeared to influence the work reported in this paper.

Data availability

Data will be made available on request.

Acknowledgements

Funding for this research was provided by the US National Science Foundation (NSF # ECI - 2028462) and Transportation Infrastructure Durability centre (TIDC) at the University of Maine, USA under grant number 69A3551847101. Former graduate students SK Belal Hossen, Kavya Kamasamudram, and Naveen Saladi are gratefully acknowledged for helping the authors to perform some of the experimental tasks presented in this article.

References

[1] L. Mo, F. Zhang, M. Deng, F. Jin, A. Al-Tabbaa, A. Wang, Accelerated carbonation and performance of concrete made with steel slag as binding materials and aggregates, Cem. Concr. Compos. 83 (2017) 138–145, https://doi.org/10.1016/j.cemconcomp.2017.07.018.
[2] R.I. Khan, W. Ashraf, J. Olek, Amino acids as performance-controlling additives in carbonation-activated cementitious materials, Cem. Concr. Res. 147 (2021) 1–39, https://doi.org/10.1016/j.cemconres.2021.106501.
[3] EIA, The Cement Industry is the Most Energy Intensive of All Manufacturing Industries, Today in Energy, 2013, pp. 1–2. http://www.eia.org.
[4] K.L. Scrivener, R.J. Kirkpatrick, Innovation in use and research on cementitious material, Cem. Concr. Res. (2008), https://doi.org/10.1016/j.cemconres.2007.09.025.
[5] A. Schöler, B. Lothenbach, F. Winnefeld, M. Zajac, Hydration of quaternary Portland cement blends containing blast-furnace slag, siliceous fly ash and limestone powder, Cem. Concr. Compos. 55 (2015) 374–382, https://doi.org/10.1016/j.cemconcomp.2014.10.001.
[6] M.I. Haque, R.I. Khan, W. Ashraf, H. Pendse, Production of sustainable, low-permeable and self-sensing cementitious composites using biochar, Sustain. Mater. Technol. 28 (2021) e00279, https://doi.org/10.1016/j.susmat.2021.e00279.
[7] J.G. Jang, G.M. Kim, H.J. Kim, H.K. Lee, Review on recent advances in CO2 utilization and sequestration technologies in cement-based materials, Constr. Build. Mater. 127 (2016) 762–773, https://doi.org/10.1016/j.conbuildmat.2016.10.017.

[8] C. Unluer, A. Al-Tabbaa, The role of brucite, ground granulated blastfurnace slag, and magnesium silicates in the carbonation and performance of MgO cements, Constr. Build. Mater. 94 (2015) 629–643, https://doi.org/10.1016/j.conbuildmat.2015.07.105.

[9] R.I. Khan, W. Ashraf, Effects of ground wollastonite on cement hydration kinetics and strength development, Constr. Build. Mater. 218 (2019) 150–161, https://doi.org/10.1016/j.conbuildmat.2019.05.061.

[10] S. Cheng, Z. Shui, T. Sun, R. Yu, G. Zhang, S. Ding, Effects of fly ash, blast furnace slag and metakaolin on mechanical properties and durability of coral sand concrete, Appl. Clay Sci. 141 (2017) 111–117, https://doi.org/10.1016/j.clay.2017.02.026.

[11] M.Á. Sanjuán, E. Estévez, C. Argiz, D. del Barrio, Effect of curing time on granulated blast-furnace slag cement mortars carbonation, Cem. Concr. Compos. 90 (2018) 257–265, https://doi.org/10.1016/j.cemconcomp.2018.04.006.

[12] M.S. Meddah, M.A. Ismail, S. El-Gamal, H. Fitriani, Performances evaluation of binary concrete designed with silica fume and metakaolin, Constr. Build. Mater. 166 (2018) 400–412, https://doi.org/10.1016/j.conbuildmat.2018.01.138.

[13] K. Kupwade-Patil, S.D. Palkovic, A. Bumajdad, C. Soriano, O. Büyüköztürk, Use of silica fume and natural volcanic ash as a replacement to Portland cement: micro and pore structural investigation using NMR, XRD, FTIR and X-ray microtomography, Constr. Build. Mater. 158 (2018) 574–590, https://doi.org/10.1016/j.conbuildmat.2017.09.165.

[14] S. Barbhuiya, P.L. Chow, S. Memon, Microstructure, hydration and nanomechanical properties of concrete containing metakaolin, Constr. Build. Mater. 95 (2015) 696–702, https://doi.org/10.1016/j.conbuildmat.2015.07.101.

[15] L. Mo, D.K. Panesar, Accelerated carbonation - a potential approach to sequester CO2 in cement paste containing slag and reactive MgO, Cem. Concr. Compos. 43 (2013) 69–77, https://doi.org/10.1016/j.cemconcomp.2013.07.001.

[16] V. Ferrini, C. De Vito, S. Mignardi, Synthesis of nesquehonite by reaction of gaseous CO2 with Mg chloride solution: its potential role in the sequestration of carbon dioxide, J. Hazard. Mater. 168 (2009) 832–837, https://doi.org/10.1016/j.jhazmat.2009.02.103.

[17] J. Sun, M.F. Bertos, S.J.R.R. Simons, J. Sun, M. Ferna, Kinetic study of accelerated carbonation of municipal solid waste incinerator air pollution control residues for sequestration of flue gas CO 2, Energy Environ. Sci. 1 (2008) 370–377, https://doi.org/10.1039/b804165m.

[18] S. Ahmad, R.A. Assaggaf, M. Maslehuddin, O.S.B. Al-Amoudi, S.K. Adekunle, S. I. Ali, Effects of carbonation pressure and duration on strength evolution of concrete subjected to accelerated carbonation curing, Constr. Build. Mater. 136 (2017) 565–573, https://doi.org/10.1016/j.conbuildmat.2017.01.069.

[19] W. Ashraf, Carbonation of cement-based materials: challenges and opportunities, Constr. Build. Mater. 120 (2016) 558–570, https://doi.org/10.1016/j.conbuildmat.2016.05.080.

[20] S. Goto, K. Suenaga, T. Kado, Calcium silicate carbonation products, J. Am. Ceram. Soc. 78 (1995) 2867–2872.

[21] V. Rostami, Y. Shao, A.J. Boyd, Z. He, Microstructure of cement paste subject to early carbonation curing, Cem. Concr. Res. 42 (2012) 186–193, https://doi.org/10.1016/j.cemconres.2011.09.010.

[22] L. Mo, F. Zhang, M. Deng, Mechanical performance and microstructure of the calcium carbonate binders produced by carbonating steel slag paste under CO2 curing, Cem. Concr. Res. 88 (2016) 217–226, https://doi.org/10.1016/j.cemconres.2016.05.013.

[23] R.I. Khan, M.I. Haque, W. Ashraf, S. Shah, Role of biopolymers in enhancing multiscale characteristics of carbonation-cured cementitious composites, Cem. Concr. Compos. 134 (2022), 104766, https://doi.org/10.1016/j.cemconcomp.2022.104766.

[24] R.I. Khan, S. Siddique, W. Ashraf, Effects of magnesia in semi-hydraulic and non-hydraulic calcium silicate binders during carbonation curing, Constr. Build. Mater. 338 (2022), 127628, https://doi.org/10.1016/j.conbuildmat.2022.127628.

[25] Q. Chen, W. Ding, H. Sun, T. Peng, Mineral carbonation of yellow phosphorus slag and characterization of carbonated product, Energy 188 (2019), 116102, https://doi.org/10.1016/j.energy.2019.116102.

[26] E. Gruyaert, P. Van Den Heede, N. De Belie, Carbonation of slag concrete: effect of the cement replacement level and curing on the carbonation coefficient - effect of carbonation on the pore structure, Cem. Concr. Compos. 35 (2013) 39–48, https://doi.org/10.1016/j.cemconcomp.2012.08.024.

[27] M.A. Boone, P. Nielsen, T. De Kock, M.N. Boone, M. Quaghebeur, V. Cnudde, Monitoring of stainless-steel slag carbonation using X-ray computed microtomography, Environ. Sci. Technol. 48 (2014) 674–680, https://doi.org/10.1021/es402767q.

[28] N. Li, N. Farzadnia, C. Shi, Microstructural changes in alkali-activated slag mortars induced by accelerated carbonation, Cem. Concr. Res. 100 (2017) 214–226, https://doi.org/10.1016/j.cemconres.2017.07.008.

[29] S. Pradhan, A. Chang Boon Poh, S. Qian, Impact of service life and system boundaries on life cycle assessment of sustainable concrete mixes, J. Clean. Prod. 342 (2022), https://doi.org/10.1016/j.jclepro.2022.130847.

[30] A.M. Braga, J.D. Silvestre, J. de Brito, Compared environmental and economic impact from cradle to gate of concrete with natural and recycled coarse aggregates, J. Clean. Prod. 162 (2017) 529–543, https://doi.org/10.1016/j.jclepro.2017.06.057.

[31] S. Demirel, H.Ö. Öz, M. Güneş, F. Çiner, S. Adın, Life-cycle assessment (LCA) aspects and strength characteristics of self-compacting mortars (SCMs) incorporating fly ash and waste glass PET, Int. J. Life Cycle Assess. 24 (2019) 1139–1153, https://doi.org/10.1007/s11367-018-1562-5.

[32] G. Habert, Assessing the environmental impact of conventional and “green” cement production, 2013. https://doi.org/10.1533/9780857097729.2.199.

[33] A. Sagastume Gutiérrez, J.J. Cabello Eras, C.A. Gaviria, J. Van Caneghem, C. Vandecasteele, Improved selection of the functional unit in environmental impact assessment of cement, J. Clean. Prod. 168 (2017) 463–473, https://doi.org/10.1016/j.jclepro.2017.09.007.

[34] B.L. Damineli, F.M. Kemeid, P.S. Aguiar, V.M. John, Measuring the eco-efficiency of cement use, Cem. Concr. Compos. 32 (2010) 555–562, https://doi.org/10.1016/j.cemconcomp.2010.07.009.

[35] ASTM, ASTM C305/2014 - Standard Practice for, ASTM. (2015) 1–3. https://doi.org/10.1520/C0305-14.2.

[36] K. Scrivener, R. Snellings, B. Lothenbach, A Practical Guide to Microstructural Analysis of Cementitious Materials, 2018. https://doi.org/10.1201/b19074.

[37] ASTM, ASTM 6433 Standard Practice for Roads and Parking Lots Pavement Condition Index Surveys, (2007) 1–8. https://doi.org/10.1520/C0192.

[38] ASTM C143/C143M, Standard Test Method for Slump of Hydraulic-Cement Concrete (2015) 1–4, https://doi.org/10.1520/C0143.

[39] G. Villain, M. Thiery, G. Platret, Measurement methods of carbonation profiles in concrete: thermogravimetry, chemical analysis and gammadensimetry, Cem. Concr. Res. 37 (2007) 1182–1192, https://doi.org/10.1016/j.cemconres.2007.04.015.

[40] W. Deboucha, N. Leklou, A. Khelidj, M.N. Oudjit, Hydration development of mineral additives blended cement using thermogravimetric analysis (TGA): methodology of calculating the degree of hydration, Constr. Build. Mater. 146 (2017) 687–701, https://doi.org/10.1016/j.conbuildmat.2017.04.132.

[41] ASTM C39, Compressive Strength of Cylindrical Concrete Specimens, ASTM Stand., 2015, pp. 1–7, https://doi.org/10.1520/C0039.

[42] ASTM C1202, Standard test method for electrical indication of concrete’s ability to resist chloride ion penetration, Am. Soc. Test. Mater. (2012) 1–8, https://doi.org/10.1520/C1202-12.2.

[43] C. Elements, U. Drilled, C. Cores, C.C. Specimens, H. Concrete, B. Statements, ASTM C42/C42M−16, ASTM Int., 2012.

[44] N. Otsuki, S. Nagataki, K. Nakashita, Evaluation of the AgNO3 solution spray method for measurement of chloride penetration into hardened cementitious matrix materials, Constr. Build. Mater. 7 (1993) 195–201, https://doi.org/10.1016/0950-0618(93)90002-T.

[45] Tool for Reduction and Assessment of Chemicals and Other Environmental Impacts (TRACI), 2014.

[46] G. Ye, X. Liu, G. De Schutter, A.M. Poppe, L. Taerwe, Influence of limestone powder used as filler in SCC on hydration and microstructure of cement pastes, Cem. Concr. Compos. 29 (2007) 94–102, https://doi.org/10.1016/j.cemconcomp.2006.09.003.

[47] J. Chang, Y. Gu, W.S. Ansari, Mechanism of blended steel slag mortar with CO2 curing exposed to sulfate attack, Constr. Build. Mater. 251 (2020), 118880, https://doi.org/10.1016/j.conbuildmat.2020.118880.

[48] Y. Maierdan, M.A. Haque, B. Chen, M. Maimaitiyiming, M.R. Ahmad, Recycling of waste river sludge into unfired green bricks stabilized by a combination of phosphogypsum, slag, and cement, Constr. Build. Mater. 260 (2020), 120666, https://doi.org/10.1016/j.conbuildmat.2020.120666.

[49] S.K. Singh, N. Tiwari, Jyoti, Development of sustainable ternary cementitious binder with OPC integrating calcined clay and LF slag, J. Build. Eng. 75 (2023), 107025, https://doi.org/10.1016/j.jobe.2023.107025.

[50] R.I. Khan, M. Intesarul Haque, S. Siddique, E.N. Landis, W. Ashraf, Effects of amino acids on the multiscale properties of carbonated wollastonite composites, Constr. Build. Mater. 374 (2023), 130816, https://doi.org/10.1016/j.conbuildmat.2023.130816.

[51] P.H.R. Borges, J.O. Costa, N.B. Milestone, C.J. Lynsdale, R.E. Streatfield, Carbonation of CH and C–S–H in composite cement pastes containing high amounts of BFS, Cem. Concr. Res. 40 (2010) 284–292, https://doi.org/10.1016/j.cemconres.2009.10.020.

[52] S.A. Bernal, M.C.G. Juenger, X. Ke, W. Matthes, B. Lothenbach, N. De Belie, J. L. Provis, Characterization of supplementary cementitious materials by thermal analysis, Mater. Struct. Constr. 50 (2017) 1–13, https://doi.org/10.1617/s11527-016-0909-2.

[53] W. Ashraf, J. Olek, Carbonation activated binders from pure calcium silicates: reaction kinetics and performance controlling factors, Cem. Concr. Compos. (2018), https://doi.org/10.1016/j.cemconcomp.2018.07.004.

[54] W. Ashraf, J. Olek, S. Sahu, Phase evolution and strength development during carbonation of low-lime calcium silicate cement (CSC), Constr. Build. Mater. 210 (2019) 473–482, https://doi.org/10.1016/j.conbuildmat.2019.03.038.

[55] M. Fundamentals, A. Khawam, D.R. Flanagan, Solid-state kinetic models: basics and mathematical fundamentals, J. Phys. Chem. B. 110 (2006) 17315–17328, https://doi.org/10.1021/jp062746a.

[56] W. Ashraf, J. Olek, Carbonation behavior of hydraulic and non-hydraulic calcium silicates: potential of utilizing low-lime calcium silicates in cement-based materials, J. Mater. Sci. 51 (2016) 6173–6191, https://doi.org/10.1007/s10853-016-9909-4.

[57] P. Yu, R.J. Kirkpatrick, B. Poe, P.F. McMillan, X. Cong, Structure of calcium silicate hydrate (C–S–H): near-, mid-, and far-infrared spectroscopy, 2004. https://doi.org/10.1111/j.1151-2916.1999.tb01826.x.

[58] A. Puertas, F. Fernandez-Jimenez, Mineralogical and microstructural characterisation of alkali-activated fly ash/slag pastes, Environ. - MDPI 4 (2017) 1–14, https://doi.org/10.3390/environments4030044.

[59] J. Ihli, W.C. Wong, E.H. Noel, Y.Y. Kim, A.N. Kulak, H.K. Christenson, M.J. Duer, F. C. Meldrum, Dehydration and crystallization of amorphous calcium carbonate in solution and in air, Nat. Commun. 5 (2014) 1–10, https://doi.org/10.1038/ncomms4169.

[60] Z. Shi, C. Shi, S. Wan, N. Li, Z. Zhang, Effect of alkali dosage and silicate modulus on carbonation of alkali-activated slag mortars, Cem. Concr. Res. 113 (2018) 55–64, https://doi.org/10.1016/j.cemconres.2018.07.005.
[61] M. Thiery, G. Villain, P. Dangla, G. Platret, Investigation of the carbonation front shape on cementitious materials: effects of the chemical kinetics, Cem. Concr. Res. (2007), https://doi.org/10.1016/j.cemconres.2007.04.002.
[62] A. Hidalgo, S. Petit, C. Domingo, C. Alonso, C. Andrade, Microstructural characterization of leaching effects in cement pastes due to neutralisation of their alkaline nature. Part I: portland cement pastes, Cem. Concr. Res. 37 (2007) 63–70, https://doi.org/10.1016/j.cemconres.2006.10.002.
[63] S.A. Bernal, R.M. de Gutierrez, J.L. Provis, V. Rose, Effect of silicate modulus and metakaolin incorporation on the carbonation of alkali silicate-activated slags, Cem. Concr. Res. (2010), https://doi.org/10.1016/j.cemconres.2010.02.003.
[64] I. García Lodeiro, D.E. Macphee, A. Palomo, A. Fernández-Jiménez, Effect of alkalis on fresh C–S–H gels. FTIR analysis, Cem. Concr. Res. 39 (2009) 147–153, https://doi.org/10.1016/j.cemconres.2009.01.003.
[65] S.N. Costa, V.N. Freire, E.W.S. Caetano, F.F. Maia, C.A. Barboza, U.L. Fulco, E. L. Albuquerque, DFT calculations with van der Waals interactions of hydrated calcium carbonate crystals CaCO3·(H2O, 6H2O): structural, electronic, optical, and vibrational properties, J. Phys. Chem. A. 120 (2016) 5752–5765, https://doi.org/10.1021/acs.jpca.6b05436.
[66] M. Sato, S. Matsuda, Structure of vaterite and infrared spectra, Zeitschrift Fur Krist. - New Cryst. Struct. 129 (1969) 405–410, https://doi.org/10.1524/zkri.1969.129.5-6.405.
[67] M. Palacios, F. Puertas, Effect of carbonation on alkali-activated slag paste, J. Am. Ceram. Soc. 89 (2006) 3211–3221, https://doi.org/10.1111/j.1551-2916.2006.01214.x.
[68] W. Gallagher, FTIR analysis of protein structure, Course Man. Chem. 455 (1997) 662–666.
[69] C. Shi, Steel Slag—Its production, processing, characteristics, and cementitious properties, J. Mater. Civ. Eng. 16 (2004) 230–236, https://doi.org/10.1061/(asce)0899-1561(2004)16:3(230).
[70] G. Fang, W.K. Ho, W. Tu, M. Zhang, Workability and mechanical properties of alkali-activated fly ash-slag concrete cured at ambient temperature, Constr. Build. Mater. 172 (2018) 476–487, https://doi.org/10.1016/j.conbuildmat.2018.04.008.
[71] H. Jiang, Z. Qi, E. Yilmaz, J. Han, J. Qiu, C. Dong, Effectiveness of alkali-activated slag as alternative binder on workability and early age compressive strength of cemented paste backfills, Constr. Build. Mater. (2019), https://doi.org/10.1016/j.conbuildmat.2019.05.162.
[72] A.A.S. Javid, P. Ghoddousi, M. Jaberizadeh, B. Bozorgmehr, The comparison and introducing of plate test and electrical resistance methods of determining the setting time and thixotropy of self-consolidating concrete, J. Test. Eval. (2020) 48, https://doi.org/10.1520/JTE20180326.
[73] S. Mindess, Developments in the Formulation and Reinforcement of Concrete, 2019. https://doi.org/10.1016/C2017-0-03347-5.
[74] S.P. Zhang, L. Zong, Evaluation of relationship between water absorption and durability of concrete materials, Adv. Mater. Sci. Eng. 2014 (2014), https://doi.org/10.1155/2014/650373.
[75] G. De Schutter, K. Audenaert, Evaluation of water absorption of concrete as a measure for resistance against carbonation and chloride migration, Mater. Struct. Constr. 37 (2004) 591–596, https://doi.org/10.1617/14045.
[76] M.T. Bassuoni, M.L. Nehdi, T.R. Greenough, Enhancing the reliability of evaluating chloride ingress in concrete using the ASTM C 1202 rapid chloride penetrability test, J. ASTM Int. 3 (2006), https://doi.org/10.1520/jai13403.
[77] NT Build 492, Concrete, mortar and cement-based repair materials: chloride migration coefficient from non-steady-state migration experiments, Measurement. (1999).